Semicond. Sci. Technol. **21** (2006) 254–260 doi:10.1088/0268-1242/21/3/007

Resonance ultrasonic vibration diagnostics of elastic stress in full-size silicon wafers

A Belyaev[1], O Polupan[1], S Ostapenko[1], D Hess[1] and J P Kalejs[2]

[1] University of South Florida, 4202 East Fowler Avenue, Tampa, FL 33620, USA
[2] RWE Schott Solar Inc., Billerica, MA 01821, USA

E-mail: ostapenk@eng.usf.edu

Received 3 October 2005, in final form 22 December 2005
Published 20 January 2006
Online at stacks.iop.org/SST/21/254

Abstract
A resonance vibration approach is developed to measure residual stress non-destructively in full-size multicrystalline silicon wafers used in solar cell manufacturing. This method is based on excitation of longitudinal resonance ultrasonic vibrations in the material using an external piezoelectric transducer combined with high-sensitive ultrasonic probe and data acquisition of the frequency response to make the method suitable for in-line diagnostics during wafer and cell manufacturing. Theoretical and experimental analysis of the vibration mode in single-crystal and multicrystalline silicon wafers is used to provide a benchmark reference analysis and validation of the approach.

1. Introduction

Non-contact and non-destructive monitoring of residual stress in silicon wafers is a matter of significant concern for microelectronic as well as for photovoltaic (PV) industries. Residual elastic stresses arise in the manufacture of large diameter (about 300 mm) Czochralski silicon (Cz-Si) wafers for integrated circuit application as well as in multicrystalline (mc-Si) wafers made for solar cells, and may produce mechanical defects which reduce production yield. Specifically, excess stress can generate microcracks during processing, and eventually lead to wafer breakage. There are a number of experimental techniques available to diagnose residual stress in wafers used in the semiconductor industry. These include Raman spectroscopy [1], x-ray diffraction [2] and infrared polariscopy [3]. None of these methods are suitable in their present form for rapid in-line stress diagnostics of as-grown and processed Si wafers. In the PV industry, for example, fast in-line quality control requires methods which can achieve measurement times close to 2 s per wafer to match a throughput of a solar cell production line.

An alternative approach to measure stress and assess factors which affect the mechanical quality of full-size (up to 200 mm diameter) silicon wafers was proposed in [4]. It was based on the excitation of flexural resonance ultrasonic vibrations in the wafer using an external piezoelectric transducer combined with high-speed data acquisition to provide information on the frequency response over the entire wafer area. In the case of the circular 200 mm Cz-Si, this approach allowed tracking of stresses in wafers with nanometre thick oxide and also to assess wafers with as-grown bulk defects [5]. A similar ultrasonic technique was applied to mc-Si wafers [6]. In this paper, we have modified and extended this resonance acoustic technique to include the longitudinal wafer vibrations and provide diagnostics on the elastic stress in full-size circular Cz-Si as well as square mc-Si wafers. The main emphasis of our paper is on stress diagnostics for solar-grade mc-Si wafers. We present theoretical analysis and experimental data on Cz-Si wafers to validate our approach.

2. Experimental details

2.1. Resonance ultrasonic vibrations (RUV)

In the resonant ultrasonic method, ultrasonic vibrations of a tunable frequency and adjustable amplitude are applied to the entire silicon wafer. Ultrasonic vibrations are generated in the wafer using a resonance piezoelectric transducer. The transducer contains a central hole which provides a reliable vacuum coupling between the wafer and the transducer by applying a small (∼50 kPa) negative pressure to the backside of the wafer (figure 1).

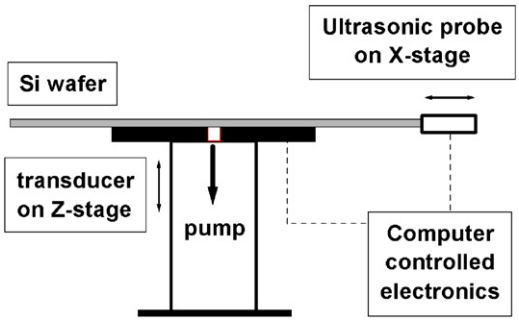

Figure 1. Schematic of the experimental set-up for resonance ultrasonic vibrations.

Ultrasonic vibrations are propagated into the wafer from the transducer and form standing acoustic waves at specific resonance frequencies. This vacuum method to couple the wafer and transducer allows fast wafer exchange and provides simple wafer alignment within 100 μm accuracy. The amplitude and spatial distribution of the standing waves are measured using a broadband ultrasonic probe. In the present design, the ultrasonic probe measures the longitudinal vibration mode characteristics by contacting the edge of the wafer with a controlled force. The resonance frequency of the longitudinal vibration mode is independent on the wafer thickness (h), in contrast to the flexural vibration mode, which is proportional to $h^{3/2}$ [7]. This is especially beneficial in mc-Si ribbon wafers which may have significant thickness variations of up to 20% across the wafer, as well as from wafer to wafer. The RUV system is computer controlled to achieve fast data acquisition and analysis.

2.2. Scanning acoustic microscopy (SAM)

Prior to wafer diagnostics using the RUV technique, each wafer is screened using a scanning acoustic microscopy (SAM) [8] to ensure that there are no peripheral microcracks that could interfere with the vibration data. In SAM, a focused high-frequency acoustic beam operating in a pulsed mode is scanned over the front surface of the wafer. These pulses are transmitted through the Si wafer at the sound velocity and are reflected at various interfaces, including the front and back surfaces of the wafer. The high-frequency acoustic waves are attenuated quickly in air, so the wafers have to be placed in a coupling medium which is deionized water in our case. The system uses the pulse echo technique and operates at frequencies up to 250 MHz. The pulse repetition rate is set at 20 kHz, so echoes from one pulse do not overlap those from the next. The reflected beam is received by the transducer and converted back to a voltage. The voltage data are amplified and digitized, providing peak amplitude, peak phase and 'time-of-flight' (TOF) data. The TOF represents the time required for a pulse to travel back and forth across the wafer thickness. TOF data were further used to obtain thickness maps on mc-Si wafers. We used a typical value for the longitudinal speed of sound in silicon of 8600 m s^{-1} to calculate the thickness. Each map was measured over a full 100 mm $\times$ 100 mm wafer area, with a step size of 50 μm. Steps as small as 5 μm can also be used for high-resolution imaging, although this significantly increases the data acquisition time.

2.3. Linear infrared polariscopy

To characterize and quantify the level and spatial distribution of in-plane stresses in the material, we have used a scanning linear infrared (IR) polariscopy technique [3]. In linear IR polariscopy, a collimated light from a 75 W halogen tungsten lamp can be focused from a 1 mm diameter down to 60 μm. The intensity of the optical transmission is measured at a 1.3 μm wavelength corresponding to a spectral region where Si is transparent. Additionally, two infrared linear polarizers are used and oriented with respect to a pre-selected crystal direction, such as the growth direction of the mc-Si ribbon. One of them (the polarizer) is located in front of the sample and the other (the analyser) immediately behind the sample. The polarization intensity is measured at selected orientations of the polarizer and analyser and depends on the optical retardation parameter, which in turn is directly related to the value of the residual elastic stress. In general, the intensity of polarization transmission can be expressed as follows:

$$I = I_0(1-R)^2[\cos^2\chi - \sin 2(\varphi-\psi) \times \sin 2(\varphi-\psi+\chi)\sin^2\delta/2], \quad (1)$$

where I_0 is the intensity of incident light, R is the reflectivity, ψ is the principal angle which determines the orientation of the strain axis at the plane, χ is the angle between polarizer and analyser, and φ is the azimuth angle of the polarizer. Equation (1) and appropriate Cartesian coordinates with angles definition can be found in [3].

The polarization intensity, I, measured at selected orientations of the polarizer and analyser, depends on the optical retardation parameter δ. To derive the relationship between δ and stress components, the following algorithm is applied. Two transmitted intensities of the polarized light are measured: one with polarizer and analyser parallel to each other, $I_\parallel = I$ ($\chi = 0$), and the other when the polarizer is orthogonal to the analyser, $I_\perp = I$ ($\chi = \pi/2$). By measuring the angular φ-dependence of the ratio $I_\perp/(I_\parallel + I_\perp)$, one can determine quantitatively the optical retardation, δ, and the direction of the principal stress angle, ψ, using the equation

$$I_\perp/(I_\parallel + I_\perp) = \sin^2 2(\varphi-\psi)\sin^2\delta/2. \quad (2)$$

As the last step of the analysis, two strain components, $|u_{zz}-u_{xx}|$ and $|u_{xz}|$, can be calculated. The first term represents a difference in tensile strains along the crystallographic Z and X directions, while the second term is the shear strain component between Z and X. The following can be used for calculating strains:

$$|u_{zz}-u_{xx}| = \left(\lambda/\pi d n_0^3\right)[\delta/(p_{11}-p_{12})]\cos(2\psi), \quad (3a)$$

$$|u_{xz}| = \left(\lambda/\pi d n_0^3\right)(\delta/p_{44})\sin 2\psi, \quad (3b)$$

where p_{ij} are photoelastic constants, d is the sample thickness and n_0 is the refractive index of the unstrained material. In the case of EFG-Si wafers, the following values were used: $\lambda = 1.3$ μm, $n_0 = 3.5$, $p_{11} = 0.081$, $p_{12} = 0.001$, $p_{44} = 0.075$. Strain components can be converted to matching values of stress using elastic constants of silicon: $c_{11} = 1.657 \times 10^{12}$ dyn cm^{-2}, $c_{12} = 0.639 \times 10^{12}$ dyn cm^{-2}, $c_{44} = 0.7956 \times 10^{12}$ dyn cm^{-2} [9].

Table 1. The set of first roots of equation (11).

m	1	2	3	4	5	6	7	8	9	10
β_m	2.049	5.389	8.572	11.732	14.862	18.025	21.173	24.318	27.463	30.612

2.4. Silicon wafer selection

Two types of silicon wafers have been included in this study. The first type is circular single crystalline Cz-Si wafers of three different diameters of 150, 200 and 300 mm, which are typically used in the microelectronic industry. The second type is square mc-Si ribbon wafers produced by the edge-defined film-fed growth (EFG) technique used in solar cell manufacture. A set of twelve 100 × 100 mm as-grown EFG wafers with thicknesses between 340 and 370 μm was chosen for this study.

3. Czochralski silicon (Cz-Si)

We first implement the resonance ultrasonic methodology for circular single-crystal silicon wafers. These wafers have typically internal stress values below 1 MPa and can serve here as model objects allowing solving analytically a general equation of the free longitudinal vibrations and to calculate resonance vibration frequencies. The vibration problem will be solved analytically and also with finite-element analysis (FEA) modelling in a simplest isotropic approximation, keeping in mind that single crystalline silicon with the diamond crystal lattice exhibits a noticeable anisotropy of elastic constants, c_{ij} as indicated in the previous paragraph. This leads, in particular, to a noticeable ∼8% variation of the sound velocity between ⟨1 1 0⟩ and ⟨1 0 0⟩ crystal directions. However, this assumption allowed a correct assignment of the experimental symmetric vibration modes leading to a small deviation with theoretical results as presented in table 2.

3.1. Modelling

We consider pure radial vibrations in a thin circular plate with radius R and thickness h, assuming that $h \ll R$. The equations for elastic strain, u_{ij}, and stress, σ_{ij}, tensors' components in the Cartesian coordinate system can be written as follows [10]:

$$\begin{cases} u_{xx} = \dfrac{1}{E}(\sigma_{xx} - \nu\sigma_{yy}), \\ u_{yy} = \dfrac{1}{E}(\sigma_{yy} - \nu\sigma_{xx}), \\ u_{xy} = \dfrac{1+\nu}{E}\sigma_{xy}, \end{cases} \tag{4}$$

where E and ν are the Young modulus and the Poisson coefficient in the x–y plane, respectively. For further consideration of the longitudinal vibrations, it is convenient to rewrite (4) in polar coordinates r, θ. Let U_r and U_θ be the respective components of the strain vector $\boldsymbol{U}$. We will be interested in symmetrical radial vibrations of the plate. Then, using symmetry of the problem, these components may be written as $U_\theta = 0$, $U_r = U$. The components of u_{ij} in polar coordinates are

$$u_{rr} = \frac{\partial U}{\partial r}, \qquad u_{\theta\theta} = \frac{U}{r}, \qquad u_{r\theta} = 0. \tag{5}$$

Therefore, equations (4) in polar coordinates can be expressed as follows:

$$\begin{cases} \sigma_{rr} = \dfrac{E}{1-\nu^2}(u_{rr} + \nu u_{\theta\theta}), \\ \sigma_{\theta\theta} = \dfrac{E}{1-\nu^2}(\nu u_{rr} + u_{\theta\theta}). \end{cases} \tag{6}$$

The equation for longitudinal vibrations in polar coordinates for radial strain component can be expressed as follows:

$$\rho\frac{\partial^2 U}{\partial t^2} = \frac{\partial \sigma_{rr}}{\partial r} + \frac{\sigma_{rr} - \sigma_{\theta\theta}}{r}, \tag{7}$$

where ρ is the density of silicon. Substituting (6) in (7) and using the expressions for u_{ij} described by (5), we can apply the method of separation of the variables for equation (7). The above procedure makes (7) to take the following form:

$$r^2\frac{\mathrm{d}^2 U}{\mathrm{d}r^2} + r\frac{\mathrm{d}U}{\mathrm{d}r} + (q^2r^2 - 1)U = 0, \tag{8}$$

where

$$q = \frac{\omega}{\sqrt{\frac{E}{(1-\nu^2)\rho}}}. \tag{9}$$

Equation (8) represents the Bessel equation of the first order and one of its solutions is

$$U(r) = AJ_1(qr), \tag{10}$$

where $J_1(qr)$ is the Bessel function of the first order. Applying the free edge boundary condition, $\sigma_{rr}|_{r=R} = 0$, it yields

$$\beta J_0(\beta) - (1-\nu)J_1(\beta) = 0, \tag{11}$$

where β is a dimensionless variable and equals qR. The first ten roots (m = 1–10) of equation (11) for $\nu = 0.3$ are presented in table 1. The respective resonance frequencies of these modes, f_m, can be calculated using the following relation:

$$f_m = \frac{\beta_m}{2\pi R}\sqrt{\frac{E}{(1-\nu^2)\rho}}. \tag{12}$$

They are plotted in figure 2 for Cz-Si wafers of three diameters of 150, 200 and 300 mm. In calculations of the resonant frequency, we used the following material constants: $E = 1.67 \times 10^{12}$ dyn cm^{-2}, $\nu = 0.3$, $\rho = 2.329$ g cm^{-3}.

3.2. Experimental results on circular Cz-Si

The calculated frequencies of the first three vibration modes are in a good agreement with RUV data on the (1 0 0)-oriented 300 mm Cz-Si wafer (figure 3). There are also a number of other resonant frequencies shown in figure 3 which are generated by asymmetric longitudinal vibrations.

Table 2 compares the first three theoretically predicted resonant frequencies for the 300 mm wafer to the experimentally measured resonant frequencies. Finite-element analysis (FEA) has also been employed to compare experimentally obtained data with theory. The FEA data are also presented in table 2.

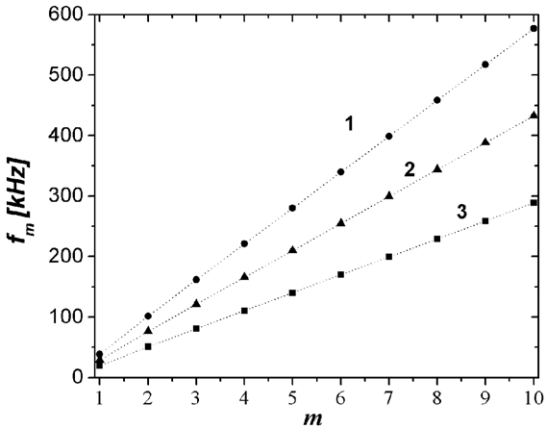

Figure 2. Normal frequencies of the longitudinal vibrations in circular silicon wafers of different diameters: (1) 150 mm, (2) 200 mm and (3) 300 mm.

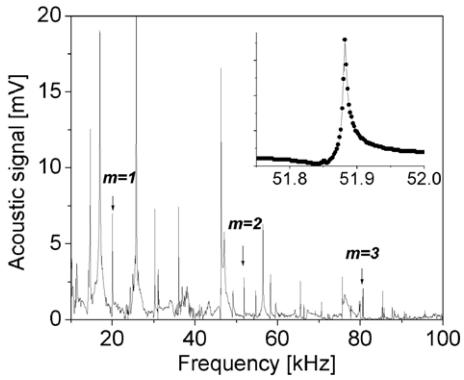

Figure 3. Frequency scan measured on the 300 mm Cz-Si wafer with first three radial modes indicated by arrows. The inset zooms in the mode for $m = 2$.

Table 2. Resonant frequencies (Hz) of radial angular independent longitudinal vibrations measured experimentally on the 300 mm diameter Cz-Si wafer compared to calculated using equation (12) and modelled with finite-element analysis (ANSYS).

m	Experiment	Theory	FEA
1	20 071	19 425	19 297
2	51 809	51 063	50 760
3	80 688	81 224	80 734

As one can see, the measured, analytically calculated and FEA modelled resonant frequencies are well correlated with deviations of less than 1%. A small difference between calculated and FEA data can be attributed to 1 mm × 1 mm size of the mesh grid used in the FEA computer modelling. The grid size matches to smallest step we used for stress mapping in multicrystalline Si wafers (see the next paragraph). We anticipate this difference to be reduced using smaller mesh grid size. This reasonable correspondence between the experimental data, theory and modelling confirms a validity of the simple model we have applied for the vibration mode analysis in circular-shaped wafers. We anticipate some deviation of the experimental data caused by the silicon crystal anisotropy in the (1 0 0) plane as discussed before and also because of the coupling of the Si wafer with the ultrasonic transducer and ultrasonic probe, which causes perturbation to the free wafer vibration spectrum. It is interesting to note a narrow bandwidth (BW) of the radial modes which can be quantified by introducing the damping ratio $\zeta_m = \mathrm{BW}/2f_m$. For first three modes, the damping ratio is equal to $\zeta_1 = 1 \times 10^{-3}$, $\zeta_2 = 1 \times 10^{-4}$ and $\zeta_3 = 2.5 \times 10^{-4}$. These low values of the acoustic damping favour using RUV metrology for quality assessment of the crystalline Si wafers.

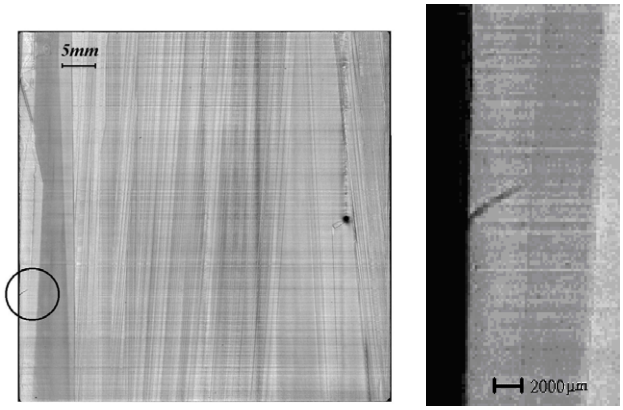

(*a*) (*b*)

Figure 4. SAM image of the 100 mm × 100 mm EFG wafer with periphery crack: (*a*) image of the entire wafer, the crack is circled at the wafer's periphery; (*b*) zooming area of the crack with 5 μm step.

4. Multicrystalline silicon

To study longitudinal vibrations in square-shaped wafers using the RUV technique, twelve 100 mm × 100 mm mc-Si EFG wafers with thicknesses ranging from 340 to 370 μm and a set of 125 mm × 125 mm cast wafers were screened using a high-resolution SAM technique, as described above, to check that microcracks over 10 μm length were not present at the wafer periphery. The mc-Si wafers show very inhomogeneous grain size distribution ranging from a few square millimetres to square centimetres. As an example, we show in figure 4(*a*) a full image of the EFG wafer with a millimetre-size peripheral crack.

The wafer was rejected from the RUV experiments based on SAM screening. The crack initially had a length of 2 mm and eventually propagated to cause the wafer breakage. We point out that the RUV technique was recently adapted to identify Cz-Si wafers with the periphery cracks [11].

In the set of EFG wafers we measured the spatial distribution of the in-plane stress using scanning linear IR polariscopy, and stress maps of all test wafers were obtained using the algorithm described in section 2.3. Representative maps of 'low'-stress and 'high'-stress wafers are presented in figure 5. Each stress map contains 100 × 100 data points obtained with a 1 mm spatial resolution. Figure 5(*a*) shows an example of a fairly uniform stress distribution over most of the low-stress EFG wafer number 16 with stress average value of 2.8 MPa. In contrast, significant variation in residual stress within EFG wafer number 22 (average stress is 5.6 MPa) is shown in figure 5(*b*). To quantify the stress mapping, we present in figure 5(*c*) two line scans measured across the

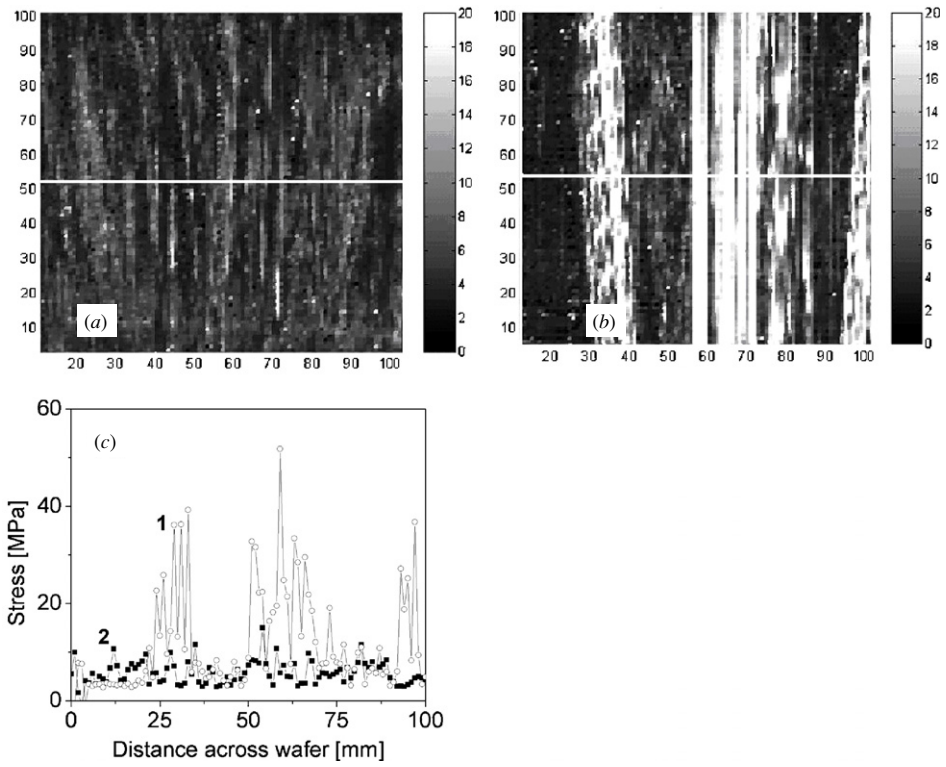

Figure 5. Stress mapping using the infrared polariscopy: (*a*) a low-stress wafer (number 16) and (*b*) high-stress wafer (number 22). Contrast bar is (MPa) values. The horizontal lines on the maps indicate the position of scan lines we have shown in (*c*), where data (1) correspond to wafer number 22 and data (2) to wafer number 16.

Table 3. Average thickness, average and peak stresses and resonance vibration frequencies of 100 mm × 100 mm EFG wafers. The wafer's thickness is used in calculation of the strain/stress values from the experimental optical retardation parameter according to equations (3*a*) and (3*b*).

Wafer ID (no)	Thickness (μm)	Average stress (MPa)	Peak stress (MPa)	Resonance frequency (kHz)
13	348	5.1	28.6	47.80
14	341	4.4	31.4	48.38
15	340	4.1	29.5	47.66
16	366	2.8	25.0	47.60
17	369	3.3	30.6	47.99
18	356	4.6	37.8	47.96
19	343	4.1	29.6	48.98
20	349	4.9	28.7	49.04
21	344	5.4	44.8	48.68
22	346	5.7	29.2	48.78
23	347	4.4	29.8	48.15
24	344	4.1	29.5	47.80

growth directions in both wafers. These show quite different stress distributions.

The values of measured wafer thickness and calculated average and peak stresses are presented in table 3. The stress values are corrected to account for the average wafer thickness, which was measured using the SAM time-of-flight technique and also confirmed by data of the wafer weight and density ($\rho_{Si} = 2.329$ g cm^{-3}).

Modal analysis of the free edge square wafer's vibrations is performed using ANSYS software package based on the finite-element method [12]. The wafer is modelled as a 100 × 100 mesh, which makes the size of individual shell element to be equal to 1 mm × 1 mm or 1.25 mm × 1.25 mm. The square wafers are modelled as an isotropic material with the Young modulus of 1.67×10^{12} dyn cm^{-2}, Poisson's coefficient of 0.3 and a density of 2.329 g cm^{-3}. Table 4 demonstrates calculated resonant frequencies of 100 mm × 100 mm and 125 mm × 125 mm square wafers compared to the experimentally measured ones. Two computed vibration modes are presented in figure 6.

Table 4. Average experimental resonance frequencies (Hz) of the three selected longitudinal vibration modes for 100 × 100 mm EFG-Si and 125 × 125 mm cast-Si wafers compared with FEA calculated values. Experimental values show standard deviation of 1% (see table 3).

100 × 100 mm EFG-Si		125 × 125 mm cast-Si	
FEA	Experiment	FEA	Experiment
48 772	48 620	39 018	41 210
60 794	62 540	48 635	49 520
85 381	88 350	59 754	60 450

Using the RUV technique described above, frequency scans (f-scans) from 10 to 100 kHz were performed on EFG wafers. We selected a dominant vibration mode at ∼48 kHz which corresponds to the mode in figure 6(*a*), in order to correlate the resonant frequencies with the respective values of the elastic stress. Two typical f-scans are shown in figure 7.

The f-scans were measured at four orthogonal sides of the square-shaped wafers and average value of the resonance peak

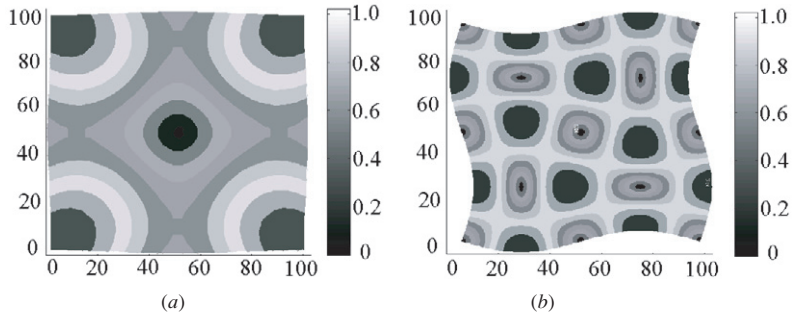

Figure 6. Finite-element analysis calculations of the first two principal mode shapes at a frequency of (*a*) 48 772 Hz and (*b*) 60 794 Hz on 100 mm × 100 mm silicon wafers.

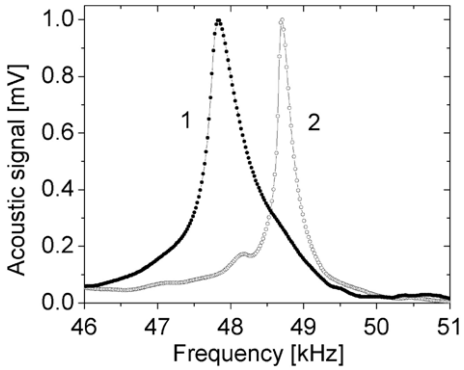

Figure 7. Normalized by intensity frequency scans at the principal maximum on two EFG wafers: (1) low-stress wafer number 16 with average stress of 5.6 MPa; (2) high-stress wafer number 22 with average stress of 2.8 MPa.

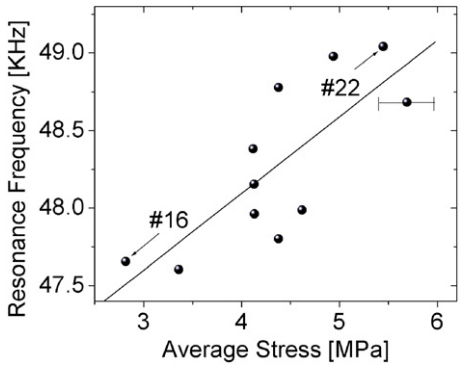

Figure 8. Experimentally measured frequencies of the resonance longitudinal vibration mode versus average stress by the infrared polariscopy technique in a set of 100 mm × 100 mm EFG wafers. Two wafers with low (number 16) and high (number 22) average stress are indicated in the graph. Note that the error bar for average stress is estimated as 0.6 MPa due to a sensitivity limit of the polariscopy set-up.

was plotted versus stress. We observe a noticeable variation of the resonance frequency on a set of identical test wafers as documented in table 3, which can be attributed to the wafer-to-wafer stress variations. In figure 8, we present the dependence of the resonance frequency on the average value of in-plane stress for these EFG wafers. Data points show a trend of a resonance frequency shift to higher values with

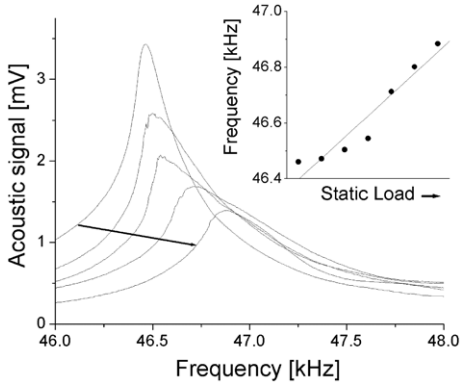

Figure 9. Frequency curves of the 46.5 kHz resonance vibration mode at different load values using five-point bending test. The arrow shows the direction of the load increase. Inset represents the resonance frequency peak upward shift with the increase of the static five-point bending stress.

the increase of the average stress in the wafer. The resonance ultrasonic mode frequency increases with increasing stress suggesting that residual stress increases wafer stiffness. We note a considerable data scattering in the frequency–stress plot (figure 8). It is conceivable to attribute this scattering to inhomogeneity and variation of grains with different wafer-to-wafer anisotropy. More experimental statistics is required to define the upward resonance frequency shift with the increase of the average stress, which may serve as a calibration curve for mechanical quality mc-Si wafer inspection.

Additional evidence of a stress-dependent resonance frequency shift is achieved from the following five-point wafer bending experiment. In this test, a cast silicon wafer was loaded vertically upwards using supporting pins applied to the four corners of the wafer while it was held in its centre with a vacuum. Concurrently, the frequency scan was taken at each loading value and the resonance vibration frequency peak location was determined (figure 9). One can see the tendency of the wafer resonance frequency location to shift to higher values with the increasing load. Our estimations of the bending stress using the ANSYS program indicate that the maximum stress values under five-point bending may be of the order of a few MPa, which is reasonably close to in-plane residual stress in as-grown EFG wafers. This loading experiment provides additional experimental evidence linking the resonant peak frequency shift to stress, as found for EFG wafers.

5. Conclusions

Resonance ultrasonic vibration methodology was developed both experimentally and theoretically and applied to the analysis of longitudinal vibrations in large diameter (up to 300 mm) circular Cz-Si and large square (up to 125 mm × 125 mm) mc-Si wafers. Specific vibration modes were identified in wafers with different geometric shapes and correlated to in-plane residual stress. In mc-Si EFG wafers, we observed a clear trend of increasing resonance frequency of the longitudinal vibration mode with higher average in-plane stress obtained with scanning IR polariscopy. This ultrasonic approach has the potential to be further developed into a diagnostic tool to address the needs of silicon wafer manufacturers, both in microelectronic and in solar cell industries.

Acknowledgment

The work was supported by National Renewable Energy Laboratory subcontract no AAT-2-31606-06.

References

[1] Gogotsi Y, Rosenberg M S, Kailer A and Nickel K G 1998 *Tribology Issues and Opportunities in MEMS* (Dordrecht: Kluwer) p 431
[2] Tanner B K 1988 *Diagnostic Techniques for Semiconductor Material and Devices* (Pennington, NJ: Electrochemical Society)
[3] Yamada M 1985 *Appl. Phys. Lett.* **47** 365
[4] Ostapenko S and Tarasov I 2000 *Appl. Phys. Lett.* **76** 2217
[5] Belyaev A, Tarasov I, Ostapenko S, Koveshnikov S, Kochelap V A and Belyaev A E 2000 *ECS Proc.* **17** 660
[6] Belyaev A, Lulu S, Tarasov I, Ostapenko S and Kalejs J P 2002 *Conference Records of 29th IEEE PVSC (New Orleans)* p 332
[7] Blevins R D 2001 *Formulas for Natural Frequencies and Mode Shapes* (Malabar, FL: Krieger)
[8] Moore T 1989 *Proc. Int. Symp. Testing and Failure Analysis* p 61
[9] Shaskolskaya M P 1982 *Akusticheskie Kristally* (Moscow: Nauka) p 49
[10] Demidenko A A, Piskovoi V N and Garadzhaev A 1992 *Ukr. J. Phys.* **37** 886
[11] Belyaev A, Polupan O, Dallas W, Ostapenko S, Hess D and Wohlgemuth J 2005 *Solid State Phenom.* **108–109** 509
[12] Cook R D 1989 *Concepts and Applications of Finite Element Analysis* (New York: Wiley)